HHS Public Access

Author manuscript

Biomaterials. Author manuscript; available in PMC 2017 March 30.

Published in final edited form as:

Biomaterials. 2014 September ; 35(29): 8297–8304. doi:10.1016/j.biomaterials.2014.06.015.

In vivo degradation of 14C-labeled porcine dermis biologic scaffold

Lisa E. Carey[a,b], **Christopher L. Dearth**[a,c], **Scott A. Johnson**[b], **Ricardo Londono**[b,d], **Christopher J. Medberry**[a,b], **Kerry A. Daly**[a,c,e], and **Stephen F. Badylak**[a,b,c,*]

[a]Department of Bioengineering, University of Pittsburgh, Pittsburgh, PA 15219, USA

[b]McGowan Institute for Regenerative Medicine, University of Pittsburgh, Pittsburgh, PA 15219, USA

[c]Department of Surgery, University of Pittsburgh, Pittsburgh, PA 15213, USA

[d]Medical Scientist Training Program, University of Pittsburgh, Pittsburgh, PA 15261, USA

[e]Department of Agriculture, GPO Box 858, Canberra ACT 2601, Australia

Abstract

Biologic scaffold materials are used for repair and reconstruction of injured or missing tissues. Such materials are often composed of allogeneic or xenogeneic extracellular matrix (ECM) manufactured by decellularization of source tissue, such as dermis. Dermal ECM (D-ECM) has been observed to degrade and remodel *in vivo* more slowly than other biologic scaffold materials, such as small intestinal submucosa (SIS-ECM). Histologic examination is a common method for evaluating material degradation, but it lacks sensitivity and is subject to observer bias. Utilization of ^{14}C-proline labeled ECM is a quantitative alternative for measuring degradation of ECM scaffolds. Using both methods, the amount of degradation of D-ECM and SIS-ECM was determined at 2, 4, and 24 weeks post-implantation in a rodent model. Results utilizing ^{14}C liquid scintillation counting (LSC) analysis showed distinct differences in degradation at the three time points. D-ECM material *in situ* stayed the same at 76% remaining from 2 to 4 weeks post-implantation, and then decreased to 44% remaining at 24 weeks. In the same time period, implanted SIS-ECM material decreased from 72% to 13% to 0%. Visual examination of device degradation by histology overestimated degradation at 2 weeks and underestimated device degradation at 24 weeks, compared to the ^{14}C method.

Keywords

Extracellular matrix; Dermis; Biomaterial degradation; ^{14}C quantification

[*]Corresponding author. Department of Bioengineering, University of Pittsburgh, 450 Technology Drive, Suite 300, Pittsburgh, PA 15219, USA. Tel.: +1 412 624 5253; fax: +1 412 624 5256.

1. Introduction

Biologic scaffold materials are used for the repair and reconstruction of injured or missing tissues such as abdominal wall [1–3] and other types of musculotendinous tissue [4–6], the lower urinary tract [7,8], and esophagus [9,10], among others [11,12]. These scaffolds are typically composed of allogeneic or xenogeneic extracellular matrix (ECM), which is produced by the decellularization of tissues including small intestine [1,5,12,13], urinary bladder [10,14,15], pericardium [16,17], dermis [18,19], and others [20,21]. Unless subjected to chemical cross-linking, these materials are rapidly infiltrated and degraded by host cells and replaced with neomatrix, ultimately resulting in formation of functional, site appropriate tissue [3,5,13]. These constructive remodeling processes are partially mediated by events that include modulation of the innate immune response [22,23], recruitment of endogenous stem and progenitor cells to the site of remodeling [24,25], release of matrix bound growth factors [26], and generation of bioactive cryptic peptides from ECM parent molecules [16,27]. All of these events are dependent, in part, upon cell mediated scaffold degradation processes [28], yet limited quantitative data is available regarding the *in vivo* degradation of biologic scaffold materials, especially those composed of porcine dermal ECM (D-ECM).

The composition and ultrastructure of ECM vary markedly between different tissues as a function of the tissue-specific mechanical properties, physiologic needs, and microenvironmental niche conditions. The composition and ultrastructure of each source tissue, and methods used to decellularize the tissue, influence the properties of the resultant ECM scaffold [21,29] and may influence the degradation profile. Compared to most other source tissues for ECM scaffold preparation, dermis is characterized by dense and compact matrix architecture [30]. Although numerous biologic scaffolds composed of human, bovine, or porcine dermis are commercially available [17,19] (Table 1), little quantitative data exists regarding the *in vivo* degradation profile of such devices.

Most studies of ECM scaffold degradation rely solely upon qualitative histomorphologic examination. However, definitive delineation of biologic scaffold ECM versus host neo-ECM during the process of scaffold remodeling is difficult at best [31–33]. A sensitive and quantitative method for determining the amount of ECM scaffold degradation over time has been described using ^{14}C-proline labeled ECM [16,27,34]. This method is based on the integration of ^{14}C-proline into the collagen triple helix structure of the source tissue. Because all ECM scaffolds are rich in collagen and ^{14}C is readily measured by liquid scintillation counting (LSC), this technique is useful for quantitatively measuring the *in vivo* degradation profile of various types of ECM scaffolds. This method has been previously used to show that the mass of an ECM scaffold composed of porcine small intestinal submucosa (SIS-ECM) decreases approximately 50% by 28 days post-implantation and is completely degraded by 75 days when used for musculotendinous [35] or lower urinary tract reconstruction [16].

The objectives of the present study are: 1) quantify the kinetics of degradation of porcine D-ECM and SIS-ECM scaffolds in a rodent soft tissue defect model with the ^{14}C method, and 2) compare ^{14}C results with those obtained by visual histologic examination.

2. Materials and methods

2.1. Overview of experimental procedure

The degradation profiles of two scaffold materials were examined in this study: dermal ECM (D-ECM) and small intestinal submucosa (SIS-ECM). Glutaraldehyde crosslinked SIS (XSIS-ECM) was used as a normalizing control, due to its resistance to host degradation. Each of the scaffold materials was prepared from both ^{14}C-labeled porcine tissues and non-radiolabeled porcine tissues. All scaffolds were implanted in an established model of abdominal wall reconstruction in rats [18] and the amount of radioactive material remaining after explant was quantified at 2, 4, and 24 weeks post-implantation. Degradation of the ^{14}C-labeled scaffolds was measured by LSC, which directly correlates to the remaining mass of the implanted scaffold [35]. Since the ^{14}C LSC method requires solubilization of the test articles, histologic examination of the same sample was not possible. Therefore, duplicate samples of each test article were made from non-labeled ECM and examined in parallel by histologic methods. Findings from the two methods were compared.

2.2. ^{14}C labeling of porcine ECM

All procedures were approved by the University of Pittsburgh Radiation Safety Committee and the Institutional Animal Care and Use Committee. All procedures complied with the National Institutes of Health Guidelines for the Care and Use of Laboratory Animals.

The methods for producing ^{14}C-labeled porcine tissue have been previously described [35]. Beginning at three weeks of age, piglets were given weekly intravenous injections of 10–30 μCi (dependent on weight) of ^{14}C-labeled proline (Amersham Life Science, Piscataway, NJ) until reaching 200 lbs, at approximately 5–6 months of age. In general, these tissues showed greater than 10^3 increase in ^{14}C content over background [35].

2.3. Biologic scaffold preparation

^{14}C and non-radiolabeled D-ECM devices were prepared as previously described [29]. Briefly, full thickness skin from the porcine dorsolateral flank was harvested immediately after euthanasia. The full thickness skin sheets were cut into 6 cm × 10 cm rectangles and subsequently split to remove subcutaneous fat, connective tissue and the overlying epidermis, leaving the reticular and papillary layers of dermis. Consecutive washes with Trypsin, hydrogen peroxide, Triton X-100 and EDTA, and peracetic acid achieved decellularization [29]. The resulting D-ECM was then lyophilized.

^{14}C and non-radiolabeled SIS-ECM devices were prepared as previously described [1,2]. Briefly, sections of porcine small intestine were mechanically abraded to remove the tunica muscularis externa and the majority of the tunica mucosa and then disinfected and decellularized in a peracetic acid and ethanol solution, followed by rinses of phosphate-buffered saline solution and deionized water [17].

To create devices of equal mass and similar dimensions, 25 layers of SIS-ECM were laminated together in a vacuum press. The vacuum press also dried the SIS-ECM devices. A subset of these 25 layer SIS-ECM devices was crosslinked with 0.25% glutaraldehyde for 12

h to create XSIS-ECM scaffolds. Devices (D-ECM, SIS-ECM, and XSIS-ECM, both ^{14}C-labeled and non-labeled) were cut to 70 mg (±5%) dry weight, with dimensions ranging from 0.8 cm to 1.5 cm by 1.0–2.0 cm, to control for the mass of the degrading material. All materials were lyophilized, individually packaged, and sterilized by ethylene oxide (16 h cycle at 50 °C in a Series 3plus EOGas Sterilizer, Anderson Sterilizers, Inc., Haw River, NC).

2.4. Surgical procedure

Thirty-six female, 6–8 week old Sprague Dawley rats (Charles River Laboratories) were divided into three groups (D-ECM, SIS-ECM, XSIS-ECM; $n = 4$ per device, per 3 time points). Bilateral, ventrolateral partial thickness defects that matched the ECM device dimensions (approximately 1.5 cm × 1.5 cm) were created as previously described [1,18]. Each animal received one ^{14}C-labeled device and one non-labeled device inlayed within the left and right-side defect, respectively (Fig. 1). Devices were matched within each animal by type of material (D-ECM, SIS-ECM, XSIS-ECM) and were sutured in place with 4-0 prolene (Ethicon, Blue Ash, OH) at each corner. Animals from each of the three groups were sacrificed at 2, 4, and 24 weeks and the devices harvested for LSC and histologic analysis.

2.5. Specimen processing and histologic analysis

The non-^{14}C-labeled devices and surrounding tissue were excised and placed in 10% neutral buffered formalin for histologic analysis. The specimens were embedded in paraffin, sectioned, and stained with H&E and Masson's Trichrome. H&E stained transverse sections were captured with Brightfield imaging across four distinct regions at 400× magnification (Nuance multispectral imaging, CRi, Cambridge, MA) (Fig. 2): center of ECM material (red boxes, $n = 3$ representative images); skin/ECM material interface (purple boxes, $n = 3$ representative images); abdominal wall/ECM material interface (blue boxes, $n = 3$ representative images); edge of ECM device (green boxes, $n = 2$ representative images). Images were taken for each explanted device at each time point, totaling $n = 12$ images for the center of ECM, the skin/ECM material interface, and the ECM/material interface at each time point, and $n = 8$ for images of the device edge at each time point. Images were randomly labeled and then scored by five blinded observers to estimate the amount of degradation and the number of cells infiltrating the ECM scaffold at each region. The number of infiltrating cells was determined by estimating the number of all cell nuclei to the closest 50 within the device (delineated by boundaries, as shown in Fig. 2). The amount of original ECM material remaining was estimated by scorers visually estimating the amount of collagen present in the field of view to the nearest 10%, within the device boundaries. The amount of degradation by histologic analysis was then compared with the quantitative value for degradation determined by LSC of ^{14}C.

The ^{14}C-labeled devices were excised from the surrounding tissue with all four sutures included to assure the entirety of the implant site was harvested. Surrounding tissue, including skeletal muscle below the device and fascia above the device was also collected. Explanted specimens were weighed, and then placed in 1 mL Solvable (PerkinElmer, Boston, MA) in 50 °C for 1–4 days, until fully dissolved. Ten mL of scintillation fluid (Ultima Gold; PerkinElmer, Boston, MA) was added to each sample, followed by placement

in the b-counter (model LS 1800; Beckman Coulter, Somerset, NJ) for ^{14}C quantification [35].

2.6. Liquid scintillation counting and analysis

LSC results were recorded as disintegrations per minute (DPM). DPM were calculated by measuring the counts per minute (CPM) and adjusting for counter efficiency using a known amount ^{14}C radiation control.

Standard curves of radiation disintegrations per minute (DPM) per mg of ^{14}C biologic scaffold material were established using D-ECM and SIS-ECM samples of known mass, ranging from 5 mg to 80 mg. SIS-ECM devices had greater ^{14}C values per unit mass than D-ECM devices, as shown by the difference in slope of the DPM per mass standard curves (Fig. 3). This difference may be due to the heterogeneous composition of the dermal tissue, which includes hair follicles and pockets of adipose tissue within the hypodermis layer that cannot be controlled for between devices with the current hand-splitting method. Heterogeneous areas of similar morphology do not exist within SIS-ECM devices. The rate of cell turnover in these tissues may also influence the amount of ^{14}C per mass of the materials. The cell turnover of small intestine is five times faster than the cell turnover in dermis [36], which may allow for more incorporation of ^{14}C into the SIS-ECM. These standard curves of DPM per unit mass were used to calculate the remaining amount of ^{14}C material in explanted devices.

To determine the amount of the variation within dermal source material, non-implanted ^{14}C-labeled D-ECM devices of equal mass were evaluated for ^{14}C content by LSC. The difference between the actual DPM and calculated DPM using the standard curves resulted in a 12% overall variance (Supplemental Fig. 1).

The percentage of device material remaining in each harvested specimen was determined by the difference in calculated starting DPM to DPM at the time of explant, minus the background DPM of rat abdominal wall muscle. Starting DPM was extrapolated from the starting mass of each device.

As expected, the explanted XSIS-ECM devices were not visibly degraded, as evidenced by macroscopic examination and histologic analysis (data not shown). However, LSC analysis of XSIS-ECM devices showed 80% of the device remaining compared to the starting mass at all three time points (Supplemental Fig. 2). Chemically crosslinked ECM has been shown to not degrade within 12 months [19,28]; thus, the 20% material decrease was attributed to loss of material during the XSIS-ECM implantation procedure. Small pieces from the corners of each device were typically lost during surgical implantation as a result of suture placement. The lost material therefore was not included in the DPM measurement at the time of explant, thus creating a potential source of error when comparing starting device and explant DPM. To account for this experimental variance, the amount of XSIS-ECM remaining was used as a normalizing factor for the D-ECM and SIS-ECM devices. The inclusion of a chemically crosslinked dermal ECM group was deemed to be redundant and therefore was not included.

2.7. Statistical analysis

Where appropriate, a one-way or two-way analysis of variance (ANOVA) was performed to determine significant differences with Student-Newman-Keuls post hoc testing ($p \leq 0.05$). All analyses were performed using SPSS (SPSS, Chicago, IL). Data are reported as mean ±standard deviation unless otherwise specified.

3. Results

3.1. Quantitative analysis of device degradation by LSC

LSC showed that D-ECM degraded more slowly than SIS-ECM over the time course of the study. At 2 weeks after implantation, the amount of material remaining for both D-ECM and SIS-ECM devices was approximately the same. By 4 weeks after implantation, the difference in the degradation profile between materials was striking as approximately 80% of the D-ECM material was still present, whereas only 20% of the SIS-ECM remained ($p = 0.0005$) (Fig. 4). These distinct differences in degradation remained at 24 weeks post-implantation as approximately 50% of the D-ECM scaffold material remained and the SIS-ECM was completely degraded and replaced by site appropriate host tissue.

3.2. Histologic examination of cell infiltration

The cell infiltration varied by type of device, location of the interface on the device, and time point (Fig. 5). Across all time points, less cell infiltration into the D-ECM devices was observed compared to the SIS-ECM devices (Fig. 6). Cell infiltration in the D-ECM devices was limited to the margins of the device (i.e. the edge and the device-muscle interface.) In contrast, the SIS-ECM material was readily infiltrated by cells across the entire thickness and width of the device as early as 2 weeks.

3.3. Histologic examination of material degradation

Histologic examination estimated that 60% of the D-ECM device remained at 2 weeks after implantation, with the edges of the device showing the most degradation. By 4 weeks, the estimated amount of device remaining increased to 80% D-ECM. At 24 weeks, histologic examination estimated that 20% of D-ECM remained. For SIS-ECM, 55% and 10% of the device remained after 2 and 4 weeks of implantation, as estimated by histologic examination, respectively (Fig. 7). However, at 24 weeks, the estimated amount of device remaining increased to approximately 20%. When comparing results from quantitative LSC and qualitative histologic examination, there were significant differences in amount of material remaining for both D-ECM and SIS-ECM at different time points (Fig. 8).

4. Discussion

The clinical utility of a biologic scaffold is partially dependent upon the time in which a given material is degraded and replaced by host tissue [32]. Biologic scaffold devices from dermis tissue sources are available for a variety of clinical indications (Table 1), and each material has a unique degradation profile. The degradation of scaffolds affects the mechanical properties and the host response to the scaffold, both of which affect the device

safety and utility [35]. Therefore, knowledge of the degradation characteristics for each material is critical when selecting optimal materials for each application [37].

The data presented herein support the anecdotal observations that D-ECM has a markedly slower degradation process than SIS-ECM. The prolonged degradation of D-ECM is consistent with clinical reports. Histologic examination of Strattice™ (porcine dermal ECM) used in breast reconstruction showed a minimally degraded scaffold at 6 weeks and a fully integrated scaffold by two years [38,39]. The difference in degradation between D-ECM and SIS-ECM can be attributed to a number of factors, including the composition and ultrastructure of the ECM, the amount of cell infiltration, and processing method.

ECM scaffolds are composed of structural and functional molecules secreted by the resident cells of each tissue and have tissue-specific composition and material properties [17,20]. The dermis is part of the thick defensive barrier separating the ‘outside’ and ‘inside’ of the body; accordingly, the composition and structure of the D-ECM are specific for barrier protection. The D-ECM is composed of structural proteins from the reticular and papillary layers dermis, primarily collagen type I and approximately 15% type III collagen [30,40]. D-ECM collagen fibers have a unique woven, non-uniaxial fiber orientation [40,41] and are thick and coarse compared to collagen arrangements in other tissues [42,43]. This strong, dense network of collagens hinders the degradation of D-ECM in comparison to other ECM types. In contrast, SIS-ECM is composed of thin, laminated layers [37]: the stratum compactum, muscularis mucosa, tunica submucosa. These layers are composed primarily of collagen type I, with negligible amounts of collagen types III, IV, V and VI [17] with alignment in a crisscross pattern, similar to dermis [44]; however, the SIS-ECM collagen fibers are substantially thinner than the dermal collagen fibers [45,46].

In the present study, histologic examination of implanted devices showed significantly (p-value < 0.001) less cell infiltration into D-ECM material than SIS-ECM, which correlated inversely with the amount of material degradation. These findings corroborate those of other degradation studies, in which scaffold degradation was associated with the extent and distribution of cellular infiltration [27,28,47]. While this study did not specifically identify the phenotype of cells infiltrating the scaffolds, previous studies identifying cell populations that infiltrate biologic scaffolds following implantation suggest that macrophages are the predominant cell population [48]. Macrophages are essential to material breakdown and new tissue reconstruction. Previous studies in which macrophage function was inhibited showed a lack of material degradation [28] and no new tissue remodeling [47].

Differences in processing techniques for D-ECM and SIS-ECM may also contribute to the material degradation profiles. Although the process used to decellularize dermis in this study has been optimized to be the least damaging to the D-ECM structure [29], it nonetheless utilizes detergents and enzymatic agents, which disrupt ECM ultrastructure, cross-link proteins, and remove ECM constituents such as collagen, laminin, fibronectin, elastin, and GAGs [49]. Small intestine can be effectively decellularized by mechanical delamination, a brief exposure to peracetic acid, and deionized water rinse, which results in less disruption of the natural ECM architecture [1]. Future work to investigate the effect of decellularization

and other processing methods on the degradation profile of various ECM scaffolds is warranted.

Comparison of the quantitative ^{14}C method versus histologic examination to determine ECM scaffold degradation showed that visual distinction between original ECM implant and newly deposited host ECM is difficult. The estimated amount of material remaining for the implanted devices was inaccurate for both D-ECM and SIS-ECM materials. Though visual analysis of histologic sections is commonly used to evaluate tissue remodeling [31–33], the results of the present study suggest that histologic examination alone is inadequate for determining complete the degradation profile of biologic scaffold material.

The observed degradation period of SIS-ECM in the present study is shorter than previously reported in ^{14}C degradation studies [16,27,35]. When used as a biologic scaffold for Achilles tendon, 40% of the original SIS-ECM remained at the site of remodeling after 4 weeks [27]. When placed in the urinary bladder, 60% of the original SIS-ECM remained after 4 weeks [16]. In the present study, 20% of the original the SIS-ECM remained after 4 weeks. The difference in degradation profiles may be due to rapidity and amount of cell infiltration in each anatomic location. The urinary bladder remodeling study used a single layer device [16]. The SIS-ECM device for Achilles tendon repair was made of a 10 layers of SIS-ECM that delaminated soon after implant [27]. In contrast, the device used in the present study was 25 layers, a design necessary to match the mass of D-ECM. The device in the present study similarly delaminated quickly *in vivo* and offered greater surface area for cell infiltration, with over 300 cells infiltrating per field of view in the present study, compared to 100 cells per field of view in the Achilles tendon repair study [27]. Thus, this increase in cell infiltration could account, in part, for the difference in degradation times between the studies.

5. Conclusions

Initial degradation of D-ECM occurs at the device surfaces, with limited cell infiltration into the device interior; however, D-ECM remains approximately 50% intact after 6 months *in vivo*. Qualitative methods of device degradation by histology do not correlate well with the quantitative degradation profiles and care must be taken when using this as the sole means of determining degradation of biologic scaffold materials.

Supplementary Material

Refer to Web version on PubMed Central for supplementary material.

Acknowledgments

Funding for this research was provided, in part, by C. R. Bard. Lisa Carey was partially supported by the NIH-NHLBI training grant (T32-HL76124-6) entitled “Cardiovascular Bioengineering Training Program” through the University of Pittsburgh, Department of Bioengineering. The authors would like to thank Deanna Rhoads and Lori Perez at the McGowan Histology Center for histologic section preparation. The authors would also like to thank Tim Keane, Denver Faulk, Peter Slivka, and Eve Simpson for their assistance with animal care and manuscript preparation.

Appendix A. Supplementary data

Supplementary data related to this article can be found online at http://dx.doi.org/10.1016/j.biomaterials.2014.06.015.

References

1. Badylak S, Kokini K, Tullius B, Simmons-Byrd A, Morff R. Morphologic study of small intestinal submucosa as a body wall repair device. J Surg Res. 2002; 103(2):190–202. [PubMed: 11922734]
2. Clarke KM, Lantz GC, Salisbury SK, Badylak SF, Hiles MC, Voytik SL. Intestine submucosa and polypropylene mesh for abdominal wall repair in dogs. J Surg Res. 1996; 60(1):107–14. [PubMed: 8592400]
3. Valentin JE, Turner NJ, Gilbert TW, Badylak SF. Functional skeletal muscle formation with a biologic scaffold. Biomaterials. 2010; 31(29):7475–84. [PubMed: 20638716]
4. Turner NJ, Yates AJ Jr, Weber DJ, Qureshi IR, Stolz DB, Gilbert TW, et al. Xenogeneic extracellular matrix as an inductive scaffold for regeneration of a functioning musculotendinous junction. Tissue Eng Part A. 2010; 16(11):3309–17. [PubMed: 20528669]
5. Dejardin LM, Arnoczky SP, Ewers BJ, Haut RC, Clarke RB. Tissue-engineered rotator cuff tendon using porcine small intestine submucosa. Histologic and mechanical evaluation in dogs. Am J Sports Med. 2001; 29(2):175–84. [PubMed: 11292042]
6. Mase VJ Jr, Hsu JR, Wolf SE, Wenke JC, Baer DG, Owens J, et al. Clinical application of an acellular biologic scaffold for surgical repair of a large, traumatic quadriceps femoris muscle defect. Orthopedics. 2010; 33(7):511. [PubMed: 20608620]
7. Kropp BP, Rippy MK, Badylak SF, Adams MC, Keating MA, Rink RC, et al. Regenerative urinary bladder augmentation using small intestinal submucosa: urodynamic and histopathologic assessment in long-term canine bladder augmentations. J Urol. 1996; 155(6):2098–104. [PubMed: 8618344]
8. Atala A, Freeman MR, Vacanti JP, Shepard J, Retik AB. Implantation in vivo and retrieval of artificial structures consisting of rabbit and human urothelium and human bladder muscle. J Urol. 1993; 150(2 Pt 2):608–12. [PubMed: 8326605]
9. Nieponice A, McGrath K, Qureshi I, Beckman EJ, Luketich JD, Gilbert TW, et al. An extracellular matrix scaffold for esophageal stricture prevention after circumferential EMR. Gastrointest Endosc. 2009; 69(2):289–96. [PubMed: 18657808]
10. Badylak S, Meurling S, Chen M, Spievack A, Simmons-Byrd A. Resorbable bioscaffold for esophageal repair in a dog model. J Pediatr Surg. 2000; 35(7):1097–103. [PubMed: 10917304]
11. Kelly DJ, Rosen AB, Schuldt AJ, Kochupura PV, Doronin SV, Potapova IA, et al. Increased myocyte content and mechanical function within a tissue-engineered myocardial patch following implantation. Tissue Eng Part A. 2009; 15(8):2189–201. [PubMed: 19231971]
12. Badylak SF, Lantz GC, Coffey A, Geddes LA. Small intestinal submucosa as a large diameter vascular graft in the dog. J Surg Res. 1989; 47(1):74–80. [PubMed: 2739401]
13. Musahl V, Abramowitch SD, Gilbert TW, Tsuda E, Wang JH-C, Badylak SF, et al. The use of porcine small intestinal submucosa to enhance the healing of the medial collateral ligamentea functional tissue engineering study in rabbits. J Orthop Res. 2004; 22(1):214–20. [PubMed: 14656683]
14. Atala A, Guzman L, Retik AB. A novel inert collagen matrix for hypospadias repair. J Urol. 1999; 162(3 Pt 2):1148–51. [PubMed: 10458452]
15. Brown B, Lindberg K, Reing J, Stolz DB, Badylak SF. The basement membrane component of biologic scaffolds derived from extracellular matrix. Tissue Eng Part A. 2006; 12(3):519–26.
16. Record RD, Hillegonds D, Simmons C, Tullius R, Rickey FA, Elmore D, et al. In vivo degradation of ^{14}C-labeled small intestinal submucosa (SIS) when used for urinary bladder repair. Biomaterials. 2001; 22(19):2653–9. [PubMed: 11519785]
17. Badylak SF, Freytes DO, Gilbert TW. Extracellular matrix as a biological scaffold material: structure and function. Acta Biomater. 2009; 5(1):1–13. [PubMed: 18938117]

18. Sicari B, Turner N, Badylak SF. An in vivo model system for evaluation of the host response to biomaterials. Meth Mol Biol. 2013; 1037:3–25.
19. Cornwell KG, Landsman A, James KS. Extracellular matrix biomaterials for soft tissue repair. Clin Podiatr Med Surg. 2009; 26(4):507–23. [PubMed: 19778685]
20. Wolf MT, Daly KA, Reing JE, Badylak SF. Biologic scaffold composed of skeletal muscle extracellular matrix. Biomaterials. 2012; 33(10):2916–25. [PubMed: 22264525]
21. Dequach JA, Yuan SH, Goldstein LS, Christman KL. Decellularized porcine brain matrix for cell culture and tissue engineering scaffolds. Tissue Eng Part A. 2011; 17(21–22):2583–92. [PubMed: 21883047]
22. Allman AJ, McPherson TB, Badylak SF, Merrill LC, Kallakury B, Sheehan C, et al. Xenogeneic extracellular matrix grafts elicit a TH2-restricted immune response. Transplantation. 2001; 71(11): 1631–40. [PubMed: 11435976]
23. Badylak SF, Valentin JE, Ravindra AK, McCabe GP, Stewart-Akers AM. Macrophage phenotype as a determinant of biologic scaffold remodeling. Tissue Eng Part A. 2008; 14(11):1835–42. [PubMed: 18950271]
24. Agrawal V, Johnson SA, Reing J, Zhang L, Tottey S, Wang G, et al. Epimorphic regeneration approach to tissue replacement in adult mammals. Proc Natl Acad Sci U S A. 2010; 107(8):3351–5. [PubMed: 19966310]
25. Beattie AJ, Gilbert TW, Guyot JP, Yates AJ, Badylak SF. Chemoattraction of progenitor cells by remodeling extracellular matrix scaffolds. Tissue Eng Part A. 2009; 15(5):1119–25. [PubMed: 18837648]
26. Hodde JP, Record RD, Liang HA, Badylak SF. Vascular endothelial growth factor in porcine-derived extracellular matrix. Endothelium. 2001; 8(1):11–24. [PubMed: 11409848]
27. Gilbert TW, Stewart-Akers AM, Simmons-Byrd A, Badylak SF. Degradation and remodeling of small intestinal submucosa in canine Achilles tendon repair. J Bone Joint Surg Am. 2007; 89(3): 621–30. [PubMed: 17332112]
28. Valentin JE, Stewart-Akers AM, Gilbert TW, Badylak SF. Macrophage participation in the degradation and remodeling of extracellular matrix scaffolds. Tissue Eng Part A. 2009; 15(7): 1687–94. [PubMed: 19125644]
29. Reing JE, Brown BN, Daly KA, Freund JM, Gilbert TW, Hsiong SX, et al. The effects of processing methods upon mechanical and biologic properties of porcine dermal extracellular matrix scaffolds. Biomaterials. 2010; 31(33):8626–33. [PubMed: 20728934]
30. Silver FH, Freeman JW, DeVore D. Viscoelastic properties of human skin and processed dermis. Skin research and technology. Official J Int Soc Bioeng Skin. 2001; 7(1):18–23.
31. Jenkins ED, Melman L, Desai S, Brown SR, Frisella MM, Deeken CR, et al. Evaluation of intraperitoneal placement of absorbable and nonabsorbable barrier coated mesh secured with fibrin sealant in a New Zealand white rabbit model. Surg Endosc. 2011; 25(2):604–12. [PubMed: 20652323]
32. Deeken CR, Melman L, Jenkins ED, Greco SC, Frisella MM, Matthews BD. Histologic and biomechanical evaluation of crosslinked and non-crosslinked biologic meshes in a porcine model of ventral incisional hernia repair. J Am Coll Surg. 2010; 212(5):880–8.
33. Valentin JE, Badylak JS, McCabe GP, Badylak SF. Extracellular matrix bioscaffolds for orthopaedic applications. A comparative histologic study. J Bone Joint Surg Am. 2006; 88(12): 2673–86. [PubMed: 17142418]
34. Rickey F, Elmore D, Hillegonds D, Badylak S, Record R. Regeneration of tissue about an animal-based scaffold: AMS studies of the fate of the scaffold. Nucl Instr Meth Phys Res B. 2000; 172:1097–103.
35. Gilbert TW, Stewart-Akers AM, Badylak SF. A quantitative method for evaluating the degradation of biologic scaffold materials. Biomaterials. 2007; 28(2):147–50. [PubMed: 16949150]
36. Fuchs E. The tortoise and the hair: slow-cycling cells in the stem cell race. Cell. 2009; 137(5):811–9. [PubMed: 19490891]
37. Harding, K., Kirsner, R., Lee, D., Mulder, G., Serena, T. Acellular matrices for the treatment of wounds: an expert working group review. London: Wounds International; 2010.

38. Salzberg CA, Dunavant C, Nocera N. Immediate breast reconstruction using porcine acellular dermal matrix (Strattice): long-term outcomes and complications. J Plast Reconstr Aesthet Surg JPRAS. 2013; 66(3):323–8. [PubMed: 23153519]
39. Katerinaki E, Zanetto U, Sterne GD. Histological appearance of Strattice tissue matrix used in breast reconstruction. J Plast Reconstr Aesthet Surg JPRAS. 2010; 63(12):e840–1. [PubMed: 20650694]
40. Osman OS, Selway JL, Harikumar PE, Stocker CJ, Wargent ET, Cawthorne MA, et al. A novel method to assess collagen architecture in skin. BMC Bioinforma. 2013; 14:260.
41. Yasui T, Tohno Y, Araki T. Characterization of collagen orientation in human dermis by two-dimensional second-harmonic-generation polarimetry. J Biomed Opt. 2004; 9(2):259–64. [PubMed: 15065889]
42. Meigel WN, Gay S, Weber L. Dermal architecture and collagen type distribution. Arch Dermatol Res Arch Fur Dermatol Forschung. 1977; 259(1):1–10.
43. Meyer W, Neurand K, Radke B. Collagen fibre arrangement in the skin of the pig. J Anat. 1982; 134(Pt 1):139–48. [PubMed: 7076540]
44. Gabella G. The cross-ply arrangement of collagen fibres in the submucosa of the mammalian small intestine. Cell Tissue Res. 1987; 248(3):491–7. [PubMed: 3607846]
45. Komuro T. The lattice arrangement of the collagen fibres in the submucosa of the rat small intestine: scanning electron microscopy. Cell Tissue Res. 1988; 251(1):117–21. [PubMed: 3342431]
46. Tanaka R, Fukushima S, Sasaki K, Tanaka Y, Murota H, Matsumoto T, et al. In vivo visualization of dermal collagen fiber in skin burn by collagen-sensitive second-harmonic-generation microscopy. J Biomed Opt. 2013; 18(6):61231. [PubMed: 23584485]
47. Godwin JW, Pinto AR, Rosenthal NA. Macrophages are required for adult salamander limb regeneration. Proc Natl Acad Sci U S A. 2013; 110(23):9415–20. [PubMed: 23690624]
48. Brown BN, Valentin JE, Stewart-Akers AM, McCabe GP, Badylak SF. Macrophage phenotype and remodeling outcomes in response to biologic scaffolds with and without a cellular component. Biomaterials. 2009; 30(8):1482–91. [PubMed: 19121538]
49. Crapo PM, Gilbert TW, Badylak SF. An overview of tissue and whole organ decellularization processes. Biomaterials. 2011; 32(12):3233–43. [PubMed: 21296410]

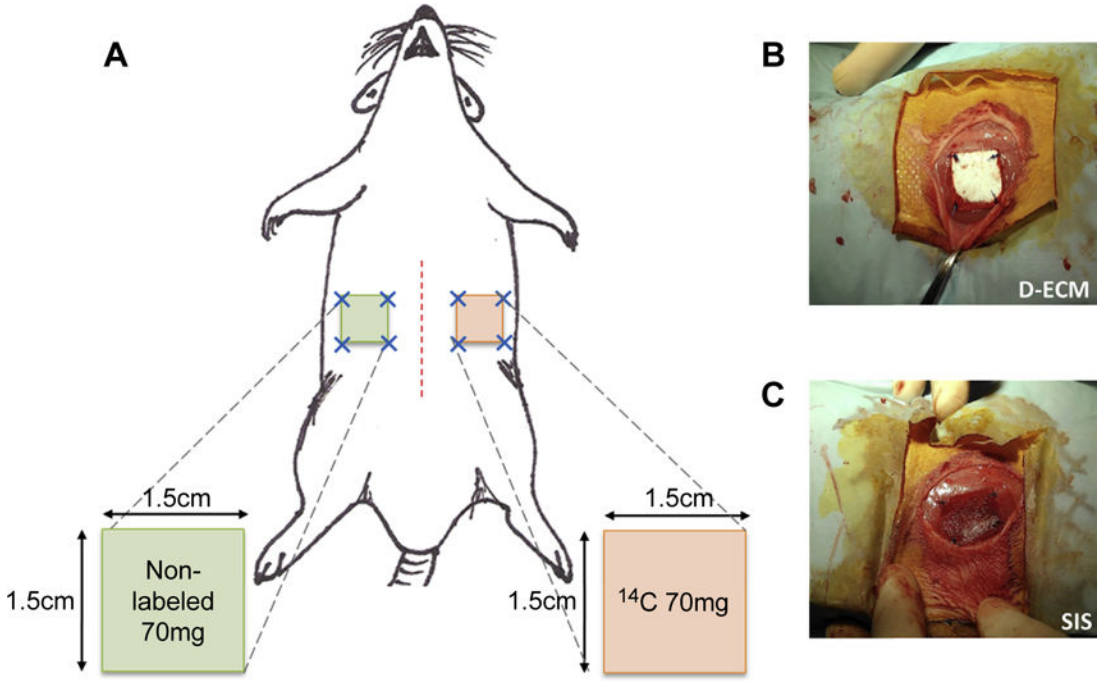

Fig. 1.

A) Schematic of bilateral abdominal implant rat model, depicting matched ^{14}C-labeled and non-radiolabeled devices. B) Implanted D-ECM devices and C) SIS-ECM devices.

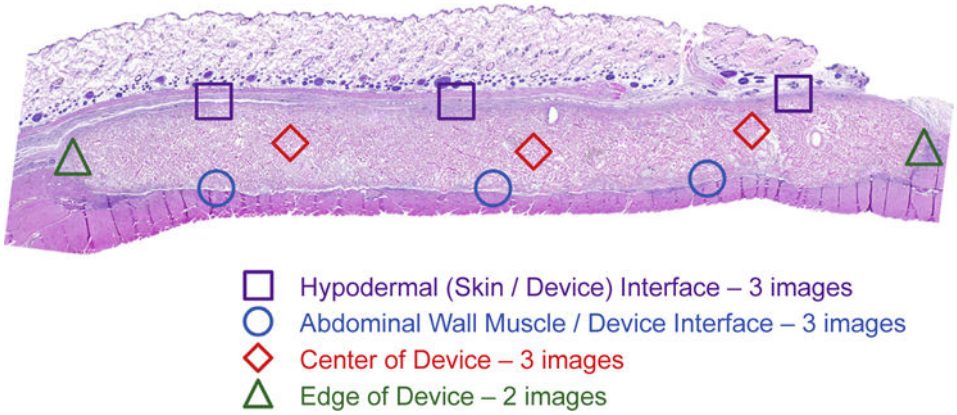

Fig. 2.

Histomorphologic Evaluation Scheme. Transverse sections were stained with H&E and eleven representative fields were imaged across four distinct regions of each tissue transverse section: center of ECM material (red diamonds); skin/ECM device interface (purple boxes); abdominal wall/ECM device interface (blue circles); edge of ECM device (green triangles). (For interpretation of the references to colour in this figure legend, the reader is referred to the web version of this article.)

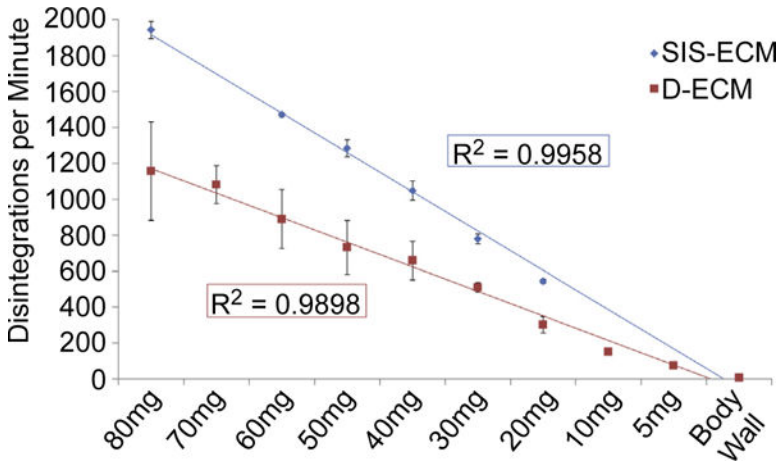

Fig. 3.

Standard curves calculating disintegrations per minute (DPM) per unit mass for D-ECM and SIS-ECM devices. Results reported as average +/− 1 standard deviation.

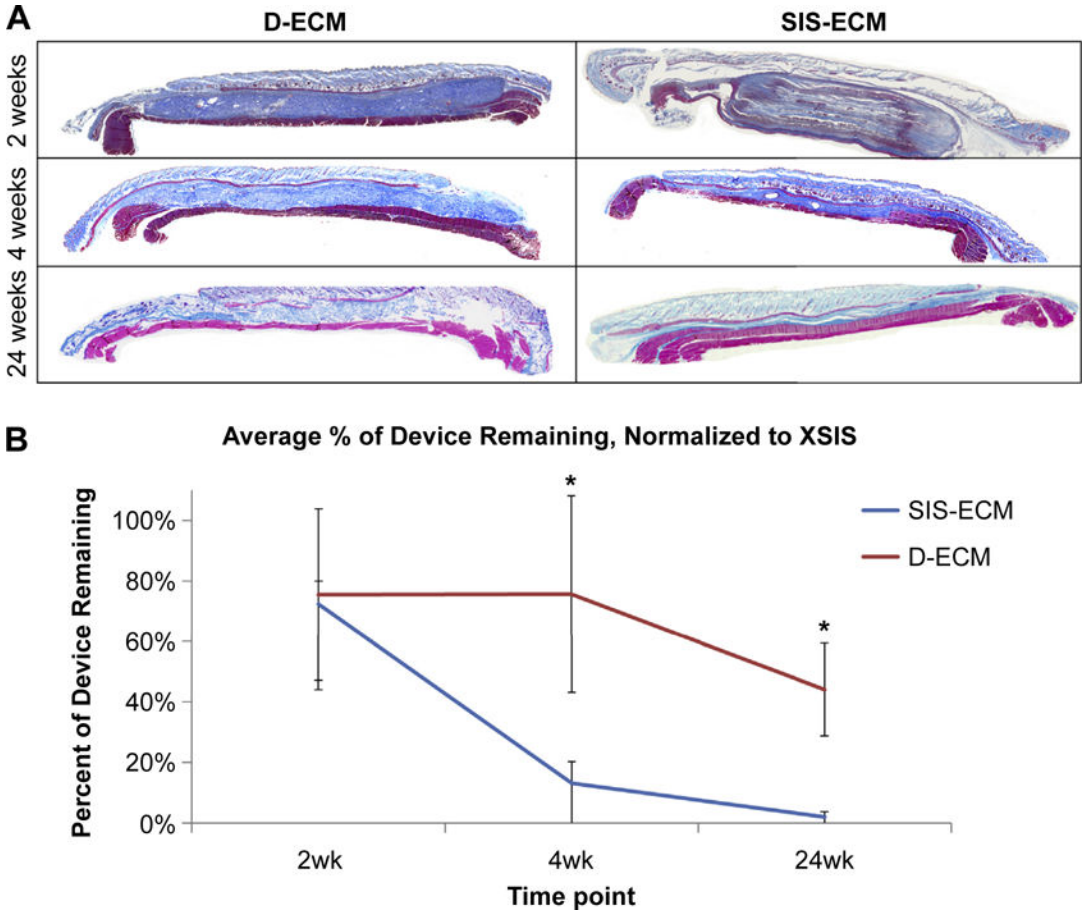

Fig. 4.

A) Representative Masson's Trichrome stained mosaic images of SIS-ECM & D-ECM at 2, 4, and 24 weeks post-implantation. B) Percent of material remaining as quantified by liquid scintillation counting (LSC), measured as a change in calculated starting disintegrations per minute (DPM) to actual measured DPM after explant, normalized to XSIS-ECM percent remaining. Results reported as average +/− 1 standard deviation. Significant differences between SIS-ECM and D-ECM at week 4 and week 24, $^{*}p$-value < 0.05.

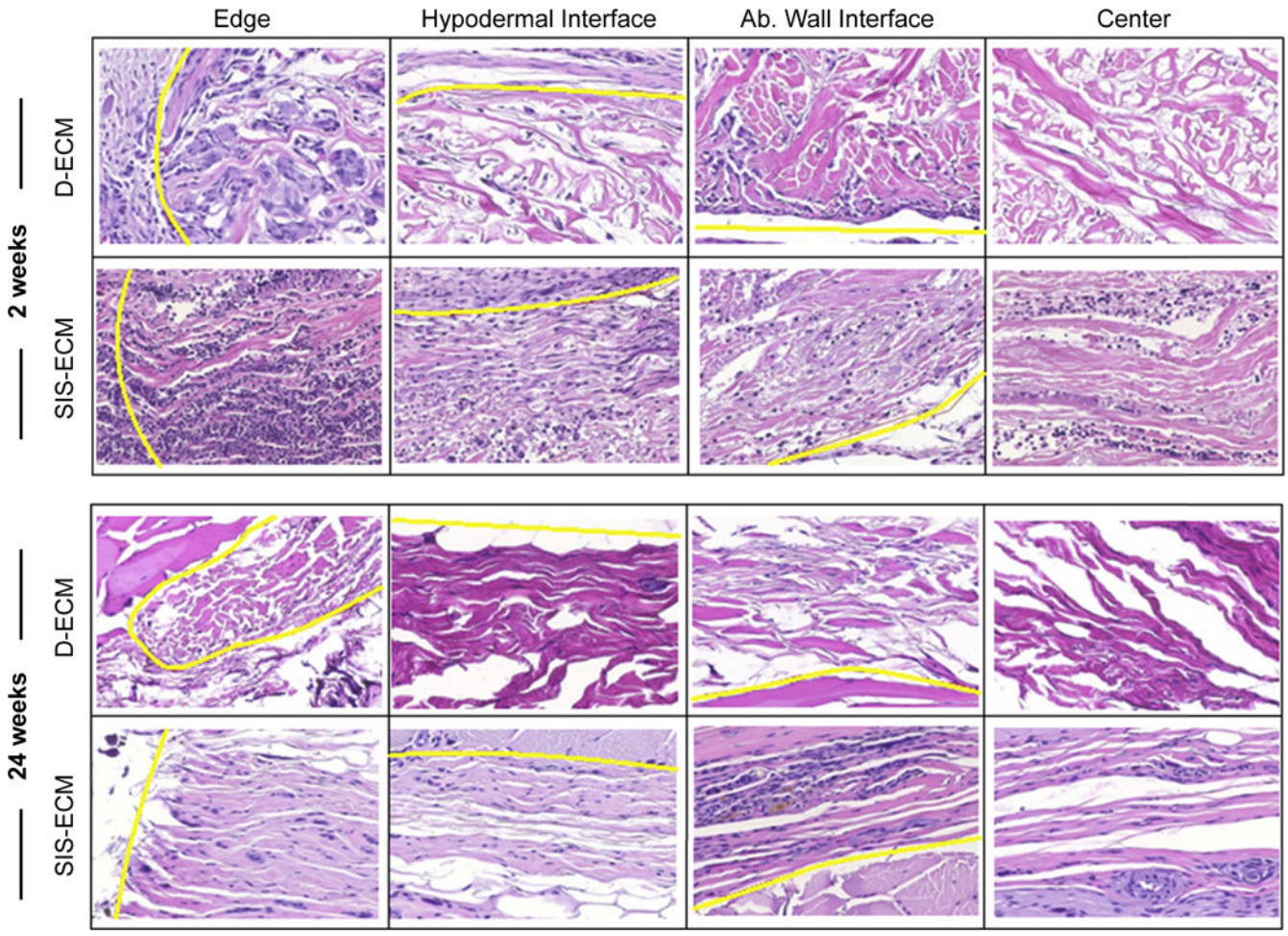

Fig. 5.

Representative H&E images of D-ECM and SIS-ECM for histologic examination, from four different device interfaces: the device edge, the hypodermal interface, the abdominal wall interface, and the center of the device. Interfaces are denoted by the yellow line. (For interpretation of the references to colour in this figure legend, the reader is referred to the web version of this article.)

A

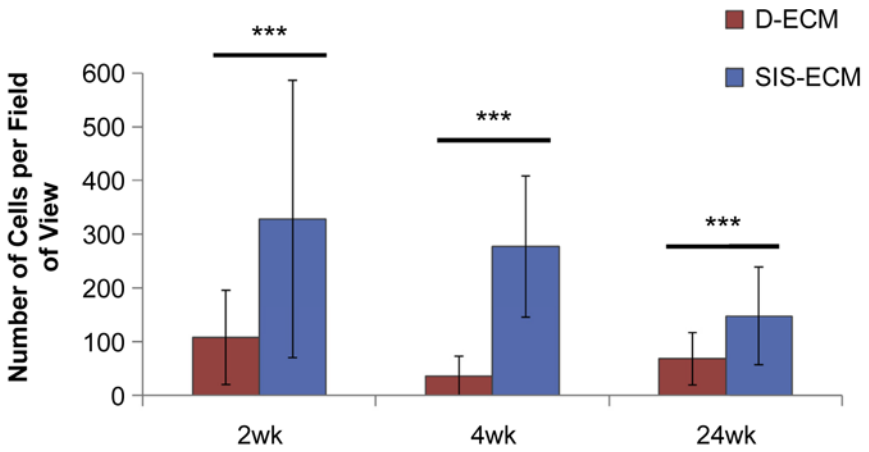

B

	D-ECM Cell Infiltration Count				SIS-ECM Cell Infiltration count			
	Device Center	Device - Muscle	Device - Skin	Edge	Device Center	Device - Muscle	Device - Skin	Edge
2wk	17 ± 18	160 ± 81	114 ± 75	159 ± 71	262 ± 250	262 ± 169	242 ± 135	656 ± 296
4wk	21 ± 31	39 ± 34	37 ± 32	54 ± 46	303 ± 143	289 ± 153	302 ± 101	185 ± 67
24wk	79 ± 69	80 ± 61	60 ± 39	58 ± 45	191 ± 147	169 ± 79	125 ± 51	134 ± 62

Fig. 6.

The number of cells counted per field of view in SIS-ECM and D-ECM devices after 2, 4, and 24 weeks of implantation. A) Comparing D-ECM to SIS-ECM overall and B) comparing different locations on the device. Results reported as average +/− 1 standard deviation. Using the independent samples Mann–Whitney *U* test, $^{***}p$-value < 0.001.

A

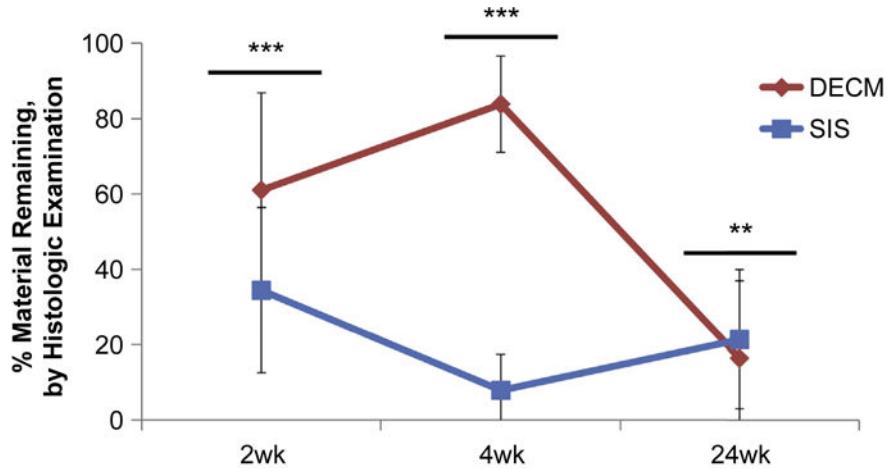

B

	D-ECM Percent of Material Remaining				SIS-ECM Percent of Material Remaining			
	Device Interior	Device – Muscle	Device - Skin	Edge	Device	Device – Muscle	Device – Skin	Edge
2wk	88 ± 11	57 ± 23	51 ± 19	41 ± 23	52 ± 26	38 ± 15	26 ± 14	16 ± 12
4wk	85 ± 21	85 ± 7	83 ± 9	83 ± 9	13 ± 12	4 ± 7	7 ± 8	7 ± 8
24wk	14 ± 18	14 ± 22	22 ± 26	13 ± 14	17 ± 14	21 ± 19	24 ± 17	26 ± 24

Fig. 7.

The percentage of material remaining by histologic examination material per field of view in SIS-ECM and D-ECM devices after 2, 4, and 24wks of implantation, A) comparing D-ECM to SIS-ECM overall and B) comparing different locations on the device. Results reported as average +/− 1 standard deviation. Using the independent samples Mann–Whitney *U* test, $^{**}p$-value < 0.01, $^{***}p$-value < 0.001.

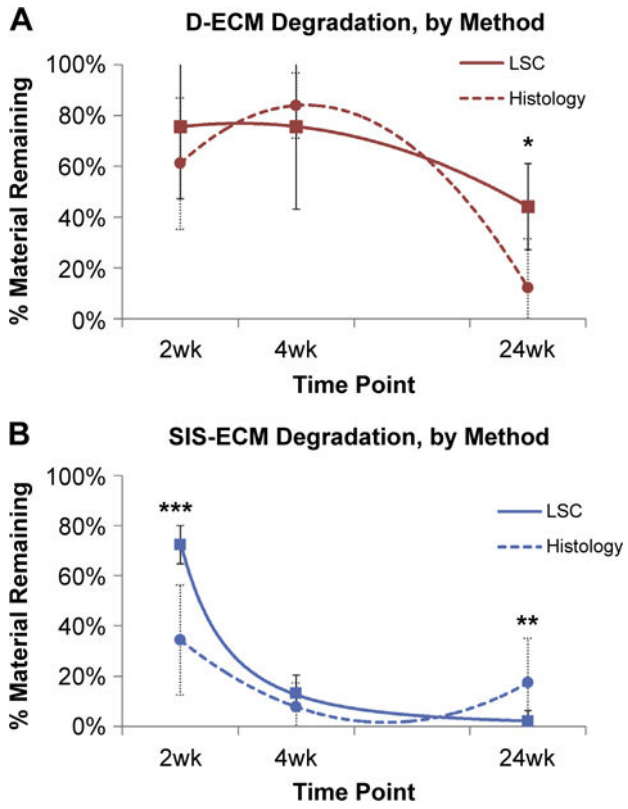

Fig. 8.

Comparison of amount of device remaining as measured by histologic examination (dotted line) or LSC (solid line) for A) D-ECM and B) SIS-ECM. Results reported as average +/− 1 standard deviation. Using independent samples Students *t*-test, $^{*}p$-value < 0.05, $^{**}p$-value < 0.01, $^{***}p$-value < 0.001.

Table 1

Commercially available biologic scaffolds composed of dermal ECM.

Product	Manufacturing company	Source of dermis	Approved indication(s)
Strattice™	LifeCell	Porcine	Hernia repair, Soft tissue reinforcement, Plastic & reconstructive surgery
Permacol™	Covidien	Porcine	Hernia repair, Plastic & reconstructive surgery
XenMatrix™	CR Bard	Porcine	Hernia repair, Plastic & reconstructive surgery
Mediskin®	Brennen Medical/Mölnlycke Health Care	Porcine	Wound healing
XCM Biologic Tissue™	Synthes	Porcine	Soft tissue reinforcement and repair, hernia repair, plastic and reconstructive surgery
Alloderm®	LifeCell	Human	Plastic reconstructive, general surgical, burn and periodontal procedures, and homologous use
Allomax™	CR Bard	Human	Hernia repair
FlexHD®	Ethicon & Musculoskeletal Transplant Foundation	Human	Homologous use
Graft Jacket®	Wright Medical Tech	Human	Homologous use
DermaSpan™	Biomet	Human	Wound coverage, plastic reconstruction, tendon reinforcement
MemoDerm™	Memometal	Human	Homologous use, wound healing
DermaMatrix™	Synthes	Human	Soft tissue grafting for dental applications
PriMatrix™	TEI Biosciences	Fetal bovine	Wound healing
SurgiMend™	TEI Biosciences	Fetal bovine	Hernia repair, plastic & reconstructive surgery
TissueMend®	TEI Biosciences	Fetal bovine	Tendon reinforcement
Xenform™	TEI Biosciences	Fetal bovine	Soft tissue reinforcement in the pelvic floor